
ADAPTIVE TUMOR GROWTH FORECASTING VIA NEURAL & UNIVERSAL ODES

A PREPRINT

Kavya Subramanian
Boston University
kavyas@bu.edu

Prathamesh Dinesh Joshi
Vizuara AI Labs
prathamesh@vizuara.com

Raj Abhijit Dandekar
Vizuara AI Labs
raj@vizuara.com

Rajat Dandekar
Vizuara AI Labs
rajatdandekar@vizuara.com

Sreedath Panat
Vizuara AI Labs
sreedath@vizuara.com

December 1, 2025

ABSTRACT

Forecasting tumor growth is critical for optimizing treatment. Classical growth models such as the Gompertz and Bertalanffy equations capture general tumor dynamics but may fail to adapt to patient-specific variability, particularly with limited data available. In this study, we leverage Neural Ordinary Differential Equations (Neural ODEs) and Universal Differential Equations (UDEs), two pillars of Scientific Machine Learning (SciML), to construct adaptive tumor growth models capable of learning from experimental data. Using the Gompertz model as a baseline, we replace rigid terms with adaptive neural networks to capture hidden dynamics through robust modeling in the Julia programming language. We use our models to perform forecasting under data constraints and symbolic recovery to transform the learned dynamics into explicit mathematical expressions. Our approach has the potential to improve predictive accuracy, guiding dynamic and effective treatment strategies for improved clinical outcomes.

Keywords Scientific Machine Learning · Neural ODE · UDE · Tumor Growth · Gompertz

1 Introduction

Cancer is among the leading causes of death worldwide [1]. In the United States alone, an estimated 2,041,910 new cancer cases and 618,120 cancer deaths *are projected to occur in 2025* [2]. Understanding cancer development and creating effective treatment strategies rely on accurately forecasting tumor growth. This is influenced by complex biological factors, including genetics, immune responses, and treatment effects, as well as environmental exposures, such as diet and radiation [3].

Traditional mathematical models based on Ordinary Differential Equations (ODEs), such as Gompertz, Bertalanffy, and logistic equations, have been widely used to describe tumor growth [4, 5, 6, 7, 8, 9, 10, 11, 12]. Although these models provide a strong theoretical foundation, they often fail to capture patient-specific variability and real-world tumor dynamics. The heterogeneity of tumor growth presents a significant challenge for fixed-parameter ODE-based models [7]. As a result, these models struggle to generalize across diverse patient populations and experimental conditions.

Researchers have utilized models based on ODEs and Partial Differential Equations (PDEs) [13] as well as some hybrid models [14] to simulate tumor dynamics. These approaches leverage well-established mathematical principles to describe tumor growth patterns. ODE-based models are computationally efficient, while PDE-based models offer spatial resolution, allowing for a more detailed representation of tumor spread. Hybrid models improve accuracy by incorporating multiple biological factors [14]. Some papers have also analyzed the interactions between tumor cells and the immune system [15, 16, 17] as well as the response to irradiation [18]. More recently, some approaches

have integrated machine learning methods to improve predictive capabilities [19]. These models excel at capturing complex, nonlinear relationships that traditional ODE and PDE models may overlook. Although pure machine learning models offer strong predictive performance, they lack interpretability and do not incorporate established biological knowledge. A model grounded in actual biology can not only provide predictions, but also provide insight into the underlying process of tumor growth [5]. In addition, these solutions cannot dynamically adapt as new patient data become available. These limitations highlight the need for a more flexible and data-driven modeling approach that allows for interpretability and adaptability.

To overcome these limitations, we employ a Scientific Machine Learning (SciML) approach that uses Neural Ordinary Differential Equations (Neural ODEs) [20] and Universal Differential Equations (UDEs) [21]. Instead of relying on fixed parameters, our approach replaces the ODE itself or key growth parameters in the ODE with neural networks. This enables the model to learn directly from experimental data, while retaining mechanistic interpretability. Our key contributions include:

- Developing Neural ODE and UDE models that adaptively learn tumor growth dynamics.
- Demonstrating robust forecasting performance under limited data
- Recovering symbolic expressions of the learned dynamics.

By combining SciML techniques with traditional tumor modeling equations, our research provides a data-driven approach that could help optimize treatment planning and enhance clinical decision-making in oncology.

2 Methodology

2.1 Data Preprocessing and Interpolation

We used a publicly available dataset [22] containing measurements of breast tumor volume in animal models. These experimental data are from studies performed on 6- to 8-week-old female mice with human LM2-4^{LUC+} triple negative breast carcinoma cells. Tumor size was measured with calipers and volume was calculated (in mm³) using the formula $V = \frac{\pi}{6}w^2L$ where L is the largest tumor diameter and w is the smallest tumor diameter.

We implemented a sigmoid-based interpolation function to construct a smooth approximation of tumor volume growth between the limited samples of experimental data. We normalized the time points between [0, 1], ensuring correct scaling to the sigmoid input range.

Figure 1 shows the sigmoid interpolation curve along with the original experimental data points for ID=1.

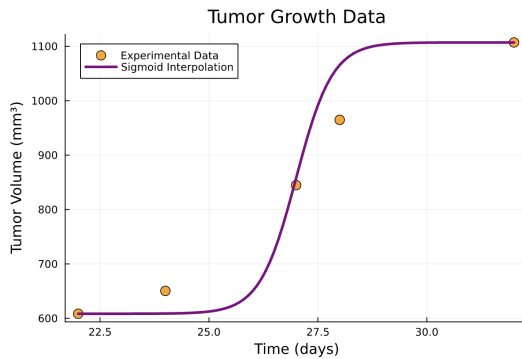


Figure 1: Experimental tumor volume measurements against the sigmoid interpolation curve.

2.2 Gompertz ODE

Tumor growth has historically been modeled using various classical mathematical models, including, but not limited to, the Bertalanffy, logistic, Gompertz, and exponential models [4, 5, 6, 7, 8, 9, 13, 23]. Although each of them has its merits, the Gompertz model, in particular, has been one of the most widely applied to describe tumor dynamics. This is due to its ability to make accurate predictions and the ease with which it fits to experimental data [5].

The Gompertz model is a sigmoidal growth model that was originally proposed by Benjamin Gompertz in 1825 to describe human mortality [24]. However, it was not until the 1960s that [25] proposed using it to model the dynamics

of tumor growth. Since then, it has been widely adopted in the biological and medical sciences for tumor modeling [4, 26, 22].

Gompertzian growth starts rapidly, then decelerates as the system approaches a maximum volume or size (known as the carrying capacity) and eventually plateaus at that value. This sigmoid-like shape is ideal, as it closely resembles the variation in tumor volume with respect to time. Mathematically, the Gompertz model is expressed as the following Ordinary Differential Equation (ODE):

$$\frac{dV}{dt} = aV \ln\left(\frac{K}{V}\right) \quad (1)$$

where:

- $V(t)$ is the tumor volume at time t ,
- a is the intrinsic growth rate,
- K is the carrying capacity, or the maximum sustainable volume.

We first modeled tumor growth dynamics using the Gompertz function, as defined in 1. The model parameters were set as the following: $a = 0.3$ and $K = 1200.0$. The ODE was solved over the experimental time span using the `TRBDF2()` solver from the `OrdinaryDiffEq.jl` package [27], with initial conditions derived from the sigmoid interpolation.

2.3 Neural ODE

To allow for greater flexibility, we implemented a Neural Ordinary Differential Equation (Neural ODE) architecture. Neural ODEs are a family of deep neural network models that use a neural network to parameterize the derivative of the hidden state [20]. They essentially use neural networks to approximate the solution of ODEs, which enables flexible modeling of continuous-time dynamics.

While traditional neural networks use discrete layers to update hidden states, Neural ODEs use a continuous transformation defined by:

$$\frac{dh}{dt} = f(h(t), t, \theta) \quad (2)$$

where:

- $h(t)$ is the hidden state at time t ,
- f is a neural network parameterized by θ ,
- the hidden state evolves according to the function f .

To ensure numerical stability and improve training convergence, the time and tumor volume data were normalized to the range $[0, 1]$ using min–max scaling. The normalized data were used as model inputs and predictions were denormalized to the original scale for visualization and evaluation.

Table 1. summarizes the key hyperparameters and model configurations used in training the Neural ODE.

Hyperparameter	Values
t_{span}	(0.0, 1.0) - normalized from (22.0, 32.0)
Random seed	Xoshiro(123)
Hidden layers	[128, 128, 64, 64]
Activation Function	tanh
Optimization Solver	Adam
Learning Rate	0.01
Number of Epochs	500

Table 1: Hyperparameter values chosen for the Neural ODE architecture.

2.4 UDE

Universal Differential Equations (UDEs) [21] combine differential equations with neural networks to efficiently model complex systems. This combination gives UDEs the interpretability and physical grounding of mechanistic models along with the adaptability of data-driven methods. This is particularly valuable when modeling systems where the dynamics are unknown or only partially known. Additionally, UDEs are ideal for applications with limited data availability, as they require fewer data points to achieve high accuracy.

We implemented a UDE by replacing the key interaction terms in the Gompertz equation with neural networks. In this approach, the Gompertz-like structure was retained, but the parameters governing the dynamics were replaced with neural networks. This resulted in the following equation:

$$\frac{dV}{dt} = NN_1 \cdot V \cdot NN_2 \quad (3)$$

where:

- NN_1 is a neural network that replaces a , and
- NN_2 is a neural network that replaces $\ln(\frac{K}{V})$

in the Gompertz equation 1

Thus, we are able to retain the known physics behind the equation while replacing the unknown components with learnable neural networks.

As in the case of the Neural ODE, the inputs were normalized for numerical stability using min-max scaling and then denormalized for visualization and evaluation.

Table 2. summarizes the key hyperparameters and model configurations used in training the UDE.

Hyperparameter	Values
t_{span}	(0.0, 1.0) - normalized from (22.0, 32.0)
Random seed	Xoshiro(123)
Hidden layers	[10, 10] each for NN_1 and NN_2
Activation Function	tanh
Optimization Solver	Adam
Learning Rate	0.01, 0.005, 0.001
Number of Epochs	1000, 1000, 500

Table 2: Hyperparameter values chosen for the UDE architecture.

2.5 Symbolic Recovery

Finally, we conducted symbolic recovery using our models to recover the hidden dynamics. After training, each model was solved to generate denormalized data. We computed their derivatives in physical space. We constructed a set of biologically-motivated basis functions to express the recovered ODE as a sparse combination of known tumor growth laws:

$$\phi_1(V) = V, \quad \phi_2(V) = V \log\left(\frac{K}{V}\right), \quad \phi_3(V) = V\left(1 - \frac{V}{K}\right), \quad \phi_4(V) = V^2$$

with the carrying capacity fixed at $K = 1200$.

We then built the design matrix ϕ using the basis functions. The coefficient vector β was estimated by solving an optimization that encourages sparsity, allowing only the most dominant basis functions to remain in the final model. The optimization was formulated and solved in Convex.jl [28] using the SCS solver.

3 Results

3.1 Gompertz ODE

Figure 2 illustrates the output of the Gompertz ODE plotted with the interpolated experimental data. The Gompertz model captures the general trend of tumor growth, characterized by a rapid initial expansion followed by deceleration

and eventual plateau. However, it exhibits noticeable deviations from the interpolated data, particularly during the mid-phase of tumor expansion. In this phase, the model significantly overestimates the tumor volume compared to the actual trend.

These discrepancies highlight a key limitation of using fixed-form mechanistic models: they lack the flexibility needed to capture the dynamics present in real tumor growth. This observation suggests that refinements to the model parameters or structure could improve performance. Alternatively, the results motivate the use of more adaptable modeling approaches, such as Neural ODEs or UDEs. These models can incorporate data-driven components to better capture complex biological behavior.

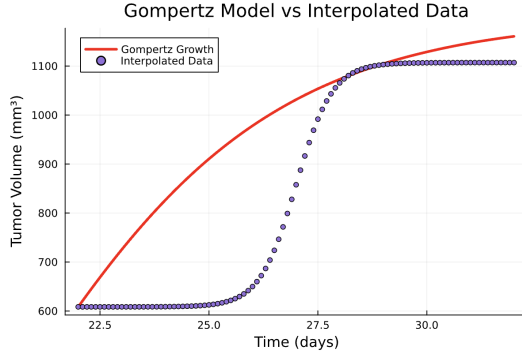


Figure 2: Solution to the Gompertz growth model against the interpolated experimental data.

3.2 Neural ODE

Figure 3 shows the solution to our Neural ODE model against the interpolated data. The model fits very well to the training data with an initial loss of 43.76308864169368 and a final optimized loss of 0.0007583699974480673.

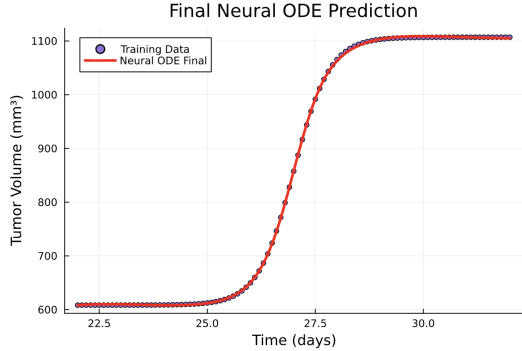


Figure 3: Solution to the Neural ODE model against the interpolated experimental data.

3.3 UDE

Figure 4 shows the solution to our Neural ODE model against the interpolated data. The model fits very well to the data with an initial loss of 250334.8665425081 and a final optimized loss of 0.9958304500732483.

3.4 Forecasting future growth

To evaluate the predictive capabilities of our models, we performed forecasting experiments using different proportions of the available data for training and the remaining portion for testing. Specifically, we trained both models using 90%, 80%, and 70% of the data and forecasted the future trajectory.

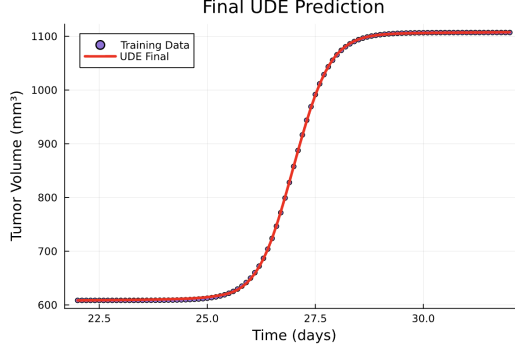


Figure 4: Solution to the UDE model against the interpolated experimental data.

3.4.1 Training with 90% of the data

Using 90% of the data for training and reserving the last 10% for forecasting, both models accurately captured the underlying growth dynamics and exhibited strong agreement with the observed data. The forecasted curves 5 closely followed the ground-truth trajectory, maintaining smooth continuity at the transition between the training and testing intervals.

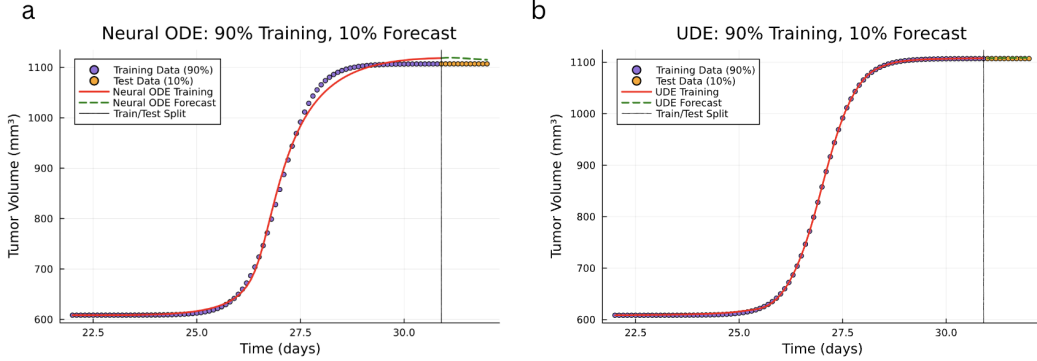


Figure 5: Forecasting using 90% of the data. (a) Neural ODE model's forecast. (b) UDE model's forecast.

3.4.2 Training with 80% of the data

With 80% of the data used for training, both models continued to perform well, maintaining strong predictive accuracy throughout the forecast window 6. In general, the results for this split were comparable to those of the 90% case, suggesting that the models remain robust even with a moderate reduction in training data.

3.4.3 Training with 70% of the data

When trained on 70% of the data, the models continued to reproduce the main growth pattern 7, although minor deviations appeared for the Neural ODE. In the case of the UDE, the training loss was higher compared to the other cases. Nevertheless, both models successfully predicted the overall trend of the system.

3.5 Symbolic Recovery

A limitation of neural networks is their black-box nature. However, by using SciML frameworks, we are able to retain the interpretability of the problem. We recovered the following equation from the Neural ODE model:

$$\frac{dV}{dt} \approx -7.8826 * V * \log(1200/V) + 11.1197 * (1 - (1/1200) * V) * V$$

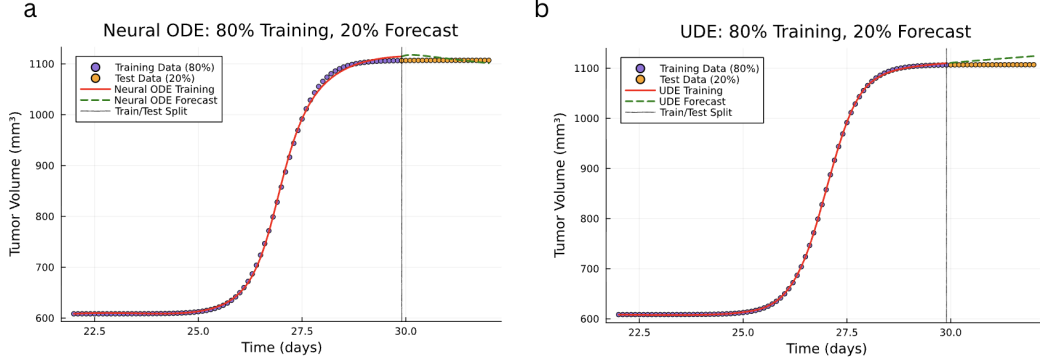


Figure 6: Forecasting using 80% of the data. (a) Neural ODE model’s forecast. (b) UDE model’s forecast.

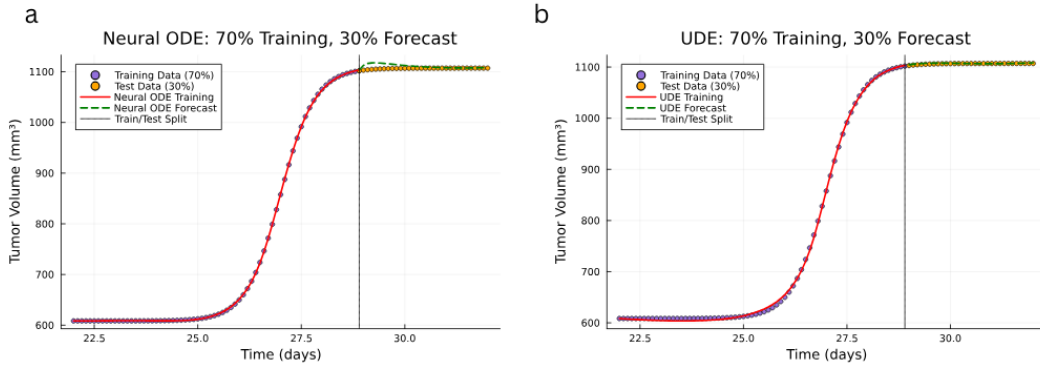


Figure 7: Forecasting using 70% of the data. (a) Neural ODE model’s forecast. (b) UDE model’s forecast.

This reveals some critical insights: The model seems to have recovered a hybrid equation that combines the Gompertz and logistic terms. The positive logistic term indicates the accelerated growth of the tumor at the initial stage. And then the negative Gompertz term shows the decline in growth as it approaches K (carrying capacity).

We recovered the following equation from the UDE model

$$\frac{dV}{dt} \approx -7.9133 * V * \log(1200/V) + 11.1575 * (1 - (1/1200) * V) * V$$

The recovered terms and their coefficients are very similar to the ones recovered by the Neural ODE.

Item	Loss value
Neural ODE	0.000758
Neural ODE 90-10	0.0270
Neural ODE 80-20	0.00475
Neural ODE 70-30	0.000228
UDE	0.996
UDE 90-10	1.51
UDE 80-20	1.16
UDE 70-30	11.3

Table 3: Summary of results including loss values for both models, forecasting with different data splits, and recovered expressions from symbolic recovery. All values given to 3 s.f.

3.6 Reproducibility Across Subjects

We reproduced these results across 10 subjects in the dataset [22]. The results are summarized in table 4.

ID	NODE Loss	UDE Loss	NODE Recovered Terms	UDE Recovered Terms
1	0.000758	0.996	$\frac{dV}{dt} \approx -7.88 * V * \log(1200/V) + 11.1 * (1 - (1/1200) * V) * V$	$\frac{dV}{dt} \approx -7.91 * V * \log(1200/V) + 11.2 * (1 - (1/1200) * V) * V$
2	0.000758	2.11	$\frac{dv}{dt} \approx -3.70 * V * \log(2100.0/V) + 6.98 * V * (1 - 0.000476V)$	$\frac{dv}{dt} \approx -3.70 * V * \log(2100.0/V) + 6.98 * V * (1 - 0.000476V)$
3	0.000758	0.864	$\frac{dv}{dt} \approx -6.36 * V * \log(1200.0/V) + 9.57 * (1 - 0.000833V) * V$	$\frac{dv}{dt} \approx -6.36 * V * \log(1200.0/V) + 9.57 * (1 - 0.000833V) * V$
4	0.000758	0.794	$\frac{dv}{dt} \approx -5.57 * V * \log(1250.0/V) + 8.76 * (1 - 0.0008V) * V$	$\frac{dv}{dt} \approx -5.57 * V * \log(1250.0/V) + 8.76 * (1 - 0.0008V) * V$
5	0.000758	0.289	$\frac{dv}{dt} \approx -8.62 * V * \log(900.0/V) + 11.7 * V * (1 - 0.00111V)$	$\frac{dv}{dt} \approx -8.62 * V * \log(900.0/V) + 11.7 * V * (1 - 0.00111V)$
6	0.000758	1.00	$\frac{dv}{dt} \approx -4.68 * V * \log(1200/V) + 7.18 * (1 - (1/1200) * V) * V$	$\frac{dv}{dt} \approx -4.68 * V * \log(1200/V) + 7.18 * (1 - (1/1200) * V) * V$
7	0.000758	0.757	$\frac{dv}{dt} \approx -6.10 * V * \log(1200/V) + 9.91 * (1 - (1/1200) * V) * V$	$\frac{dv}{dt} \approx -6.10 * V * \log(1200/V) + 9.91 * (1 - (1/1200) * V) * V$
8	0.00269	1.43	$\frac{dv}{dt} \approx -3.58 * V * \log(1350.0/V) + 6.31 * (1 - 0.000741V) * V$	$\frac{dv}{dt} \approx -2.96 * V * \log(1350.0/V) + 5.04 * (1 - 0.000741V) * V$
9	0.00269	1.06	$\frac{dv}{dt} \approx -3.58 * V * \log(1100.0/V) + 5.58 * (1 - 0.000909V) * V$	$\frac{dv}{dt} \approx -3.60 * V * \log(1100.0/V) + 5.61 * (1 - 0.000909V) * V$
10	0.00269	1.29	$\frac{dv}{dt} \approx -2.80 * V * \log(1300.0/V) + 4.90 * (1 - 0.000769V) * V$	$\frac{dv}{dt} \approx -2.82 * V * \log(1300.0/V) + 4.93 * (1 - 0.000769V) * V$

Table 4: Summary of results for ID = 1 to ID = 10 in the dataset.[22] All values given to 3 s.f.

4 Discussion

In this study, we applied SciML techniques, specifically Neural ODEs and UDEs, to model and forecast tumor growth using experimental data. Both models accurately captured the sigmoidal growth pattern that is characteristic of tumor progression. Even when trained on limited data, both models maintained stable forecasting performance, demonstrating robustness in data-scarce contexts. We also observed favorable computational performance. Both the Neural ODE and UDE architectures converged reliably during training. Training times remained modest across all subjects, suggesting that this approach is computationally feasible for real-time clinical modeling workflows.

A key aspect of this work was symbolic recovery. We extracted closed-form expressions approximating the models' learned dynamics. Across the subjects, the models recovered a positive logistic term (which could be indicative of the initial acceleration) and a negative Gompertz term (possibly suggesting the later decline). This indicates that the models were not simply learning arbitrary patterns but were capturing biologically plausible processes.

Additionally, extending the analysis across 10 subjects confirmed the reproducibility and generalizability of the approach. Our results highlight SciML as a promising framework in the field of oncology, especially for enhancing personalized cancer treatment. As the dataset included only breast tumor data, future work could examine its applicability to other tumor types, biological conditions, and treatment influences such as immune response or chemotherapy.

5 Conclusion

Our work demonstrates that Neural ODE and UDE frameworks can accurately model and forecast tumor growth by integrating mechanistic interpretability with data-driven learning. Both models captured key tumor dynamics, performed well under limited data, and produced interpretable symbolic expressions. The reproducibility across subjects underscores the robustness of the approach. By combining interpretability with adaptability, SciML provides a powerful foundation for precision oncology, enabling predictive, data-efficient, and transparent modeling of tumor growth to support personalized treatment planning.

References

- [1] World Health Organization. Cancer, 2025. URL <https://www.who.int/news-room/fact-sheets/detail/cancer>. Accessed: 2025-03-24.
- [2] Rebecca L. Siegel, Tyler B. Kratzer, Angela N. Giaquinto, Hyuna Sung, and Ahmedin Jemal. Cancer statistics, 2025. *CA: a cancer journal for clinicians*, 2025.
- [3] Philipp Altrock, Lin L. Liu, and Franziska Michor. The mathematics of cancer: Integrating quantitative models. *Nature Reviews Cancer*, 2015.
- [4] Hope Murphy, Hana Jaafari, and Hana M. Dobrovolny. Differences in predictions of ode models of tumor growth: A cautionary example. *BMC Cancer*, 2016.
- [5] Philip Gerlee. The model muddle: In search of tumor growth laws. *Cancer Research*, 2013.
- [6] Sebastien Benzekry, Clare Lamont, Afshin Beheshti, Amanda Tracz, John M. L. Ebos, Lynn Hlatky, and Philip Hahnfeldt. Classical mathematical models for description and prediction of experimental tumor growth. *PLoS Computational Biology*, 2014.
- [7] Niklas Hartung, Severine Mollard, Dominique Barbolosi, Assia Benabdallah, Guillemette Chapuisat, Gerard Henry, Sarah Giacometti, Athanassios Iliadis, Joseph Ciccolini, Christian Faivre, and Florence Hubert. Mathematical modeling of tumor growth and metastatic spreading: Validation in tumor-bearing mice. *Cancer Research*, 2014.
- [8] E. A. Sarapata and L. G. de Pillis. A comparison and catalog of intrinsic tumor growth models. *Bulletin of Mathematical Biology*, 2014.
- [9] Anyue Yin, Dirk Jan A.R. Moes, Johan G.C. van Hasselt, Jesse J. Swen, and Henk-Jan Guchelaar. A review of mathematical models for tumor dynamics and treatment resistance evolution of solid tumors. *CPT: Pharmacometrics and Systems Pharmacology*, 2019.
- [10] Samara Sharpe and Hana M. Dobrovolny. Predicting the effectiveness of chemotherapy using stochastic ode models of tumor growth. *Communications in Nonlinear Science and Numerical Simulation*, 2021.
- [11] Esmaeil Mehrara, Eva Forssell-Aronsson, Viktor Johanson, Lars Kölby, Ragnar Hultborn, and Peter Bernhardt. A new method to estimate parameters of the growth model for metastatic tumours. *Theoretical Biology and Medical Modelling*, 2013.
- [12] Esmaeil Mehrara, Eva Forssell-Aronsson, Viktor Johanson, Lars Kölby, Ragnar Hultborn, and Peter Bernhardt. A new method to estimate parameters of the growth model for metastatic tumours. *Theoretical Biology and Medical Modelling*, 2013.
- [13] Angela M. Jarrett, Ernesto A.B.F. Lima, David A. Hormuth II, Matthew T. McKenna, Xinzeng Feng, David A. Ekrut, Anna Claudia M. Resende, Amy Brock, and Thomas E. Yankeelov. Mathematical models of tumor cell proliferation: A review of the literature. *Expert Review of Anticancer Therapy*, 2018.
- [14] Ibrahim M. Chamseddine and Katarzyna A. Rejniak. Hybrid modeling frameworks of tumor development and treatment. *Wiley Interdisciplinary Reviews: Systems Biology and Medicine*, 2020.
- [15] Grace E. Mahlbacher, Kara C. Reihmer, and Hermann B. Frieboes. Mathematical modeling of tumor-immune cell interactions. *Journal of Theoretical Biology*, 2019.
- [16] Raluca Eftimie, Jonathan L. Bramson, and David J.D. Earn. Interactions between the immune system and cancer: A brief review of non-spatial mathematical models. *Bulletin of Mathematical Biology*, 2011.
- [17] Pranav Unni and Padmanabhan Seshaiyer. Mathematical modeling, analysis, and simulation of tumor dynamics with drug interventions. *Computational and Mathematical Methods in Medicine*, 2019.
- [18] Yoichi Watanabe, Erik L. Dahlman, Kevin Z. Leder, and Susanta K. Hui. A mathematical model of tumor growth and its response to single irradiation. *Theoretical Biology and Medical Modelling*, 2016.
- [19] Ana-Maria Trofin, Călin Gh. Buzea, Răzvan Buga, Maricel Agop, Lăcrămioara Ochiuz, Dragos T. Iancu, and Lucian Eva. Predicting tumor dynamics post-staged gtrs: Machine learning models in brain metastases prognosis. *Diagnostics*, 2024.
- [20] Ricky T. Q. Chen, Yulia Rubanova, Jesse Bettencourt, and David Duvenaud. Neural ordinary differential equations. *Advances in neural information processing systems*, 2018.
- [21] Christopher Rackauckas, Yingbo Ma, Julius Martensen, Collin Warner, Kirill Zubov, Rohit Supekar, Dominic Skinner, Ali Ramadhan, and Alan Edelman. Universal differential equations for scientific machine learning. *arXiv preprint arXiv:2001.04385*, 2020.

- [22] Cristina Vaghi, Anne Rodallec, Raphaelle Fanciullino, Joseph Ciccolini, Jonathan P. Mochel, Michalis Mastri, Clair Poignard, John M. L. Ebos, and Sébastien Benzekry. Population modeling of tumor growth curves and the reduced gompertz model improve prediction of the age of experimental tumors. *PLoS Computational Biology*, 2020.
- [23] Narmin Ghaffari Laleh, Chiara Maria Lavinia Loeffler, Julia Grajek, Kateřina Staňkova, Alexander T. Pearson, Hannah Sophie Muti, Christian Trautwein, Heiko Enderling, Jan Poleszczuk, and Jakob Nikolas Kather. Classical mathematical models for prediction of response to chemotherapy and immunotherapy. *PLoS Computational Biology*, 2022.
- [24] Benjamin Gompertz. Xxiv. on the nature of the function expressive of the law of human mortality, and on a new mode of determining the value of life contingencies. in a letter to francis baily, esq. f. r. s. &c. *Phil. Trans. R. Soc.*, 1825.
- [25] Anna K. Laird. Dynamics of tumour growth. *British Journal of Cancer*, 1964.
- [26] James A. Koziol, Theresa J. Falls, and Jan E. Schnitzer. Different ode models of tumor growth can deliver similar results. *BMC Cancer*, 2020.
- [27] Christopher Rackauckas and Qing Nie. Differentialequations.jl – a performant and feature-rich ecosystem for solving differential equations in julia. *Journal of Open Research Software*, 2017.
- [28] Madeleine Udell, Karanveer Mohan, David Zeng, Jenny Hong, Steven Diamond, and Stephen Boyd. Convex optimization in julia. *2014 First Workshop for High Performance Technical Computing in Dynamic Languages*, 2014.

A Summary of forecasting across subjects

ID	K	NODE 90-10	NODE 80-20	NODE 70-30	UDE 90-10	UDE 80-20	UDE 70-30
1	1200	0.0270	0.00475	0.000228	1.51	1.16	11.3
2	2100	0.0270	0.00475	0.000228	1.36	1.70	47.7
3	1200	0.0270	0.00475	0.000228	0.549	0.463	37.4
4	1250	0.0270	0.00475	0.000228	0.576	0.616	15.0
5	900	0.0270	0.00475	0.000228	0.504	1.76	6.22
6	1350	0.0270	0.00475	0.000228	0.647	1.83	25.5
7	1100	0.0270	0.00475	0.000228	0.399	0.488	14.3
8	1350	0.0401	0.00670	0.000687	0.621	3.53	31.7
9	1100	0.0401	0.00670	0.000687	0.387	0.849	17.8
10	1300	0.0401	0.00670	0.000687	0.594	3.10	29.7

Table 5: Summary of forecasting results for ID = 1 to ID = 10 in the dataset.[22] All values given to 3 s.f.

B Plots for other subjects

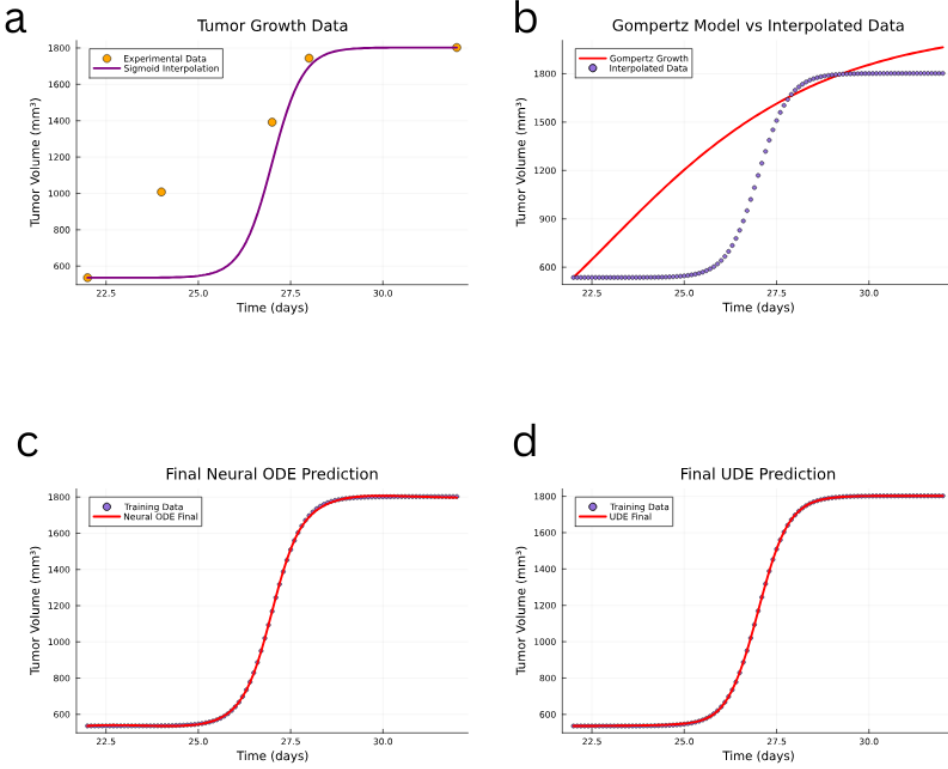


Figure 8: Plots for ID=2. (a) Sigmoid interpolation. (b) Solution to Gompertz ODE against interpolated data. (c) Solution to Neural ODE. (d) Solution to UDE.

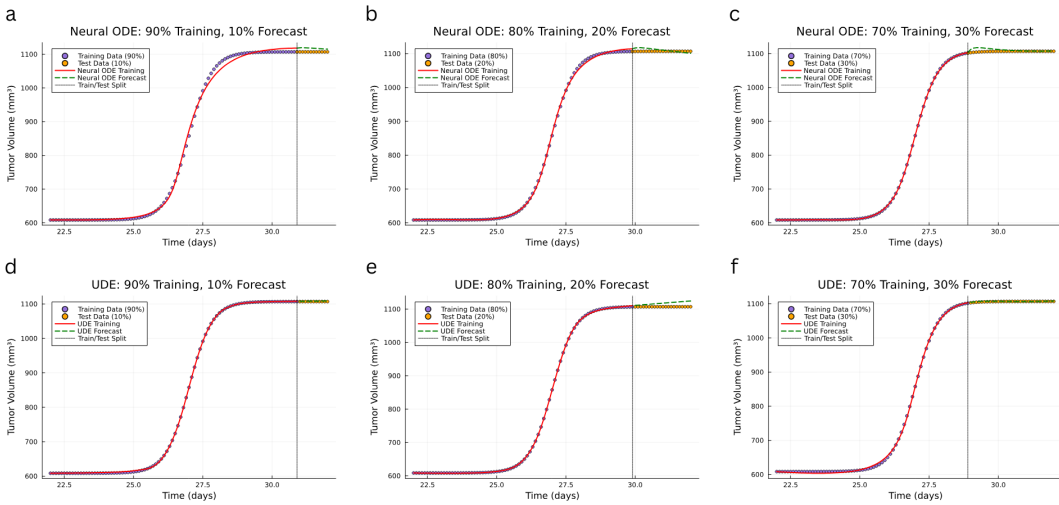


Figure 9: Forecast plots for ID=2. (a) Neural ODE forecast for 90-10 split. (b) Neural ODE forecast for 80-20 split. (c) Neural ODE forecast for 70-30 split. (d) UDE forecast for 90-10 split. (e) UDE forecast for 80-20 split. (f) UDE forecast for 70-30 split.

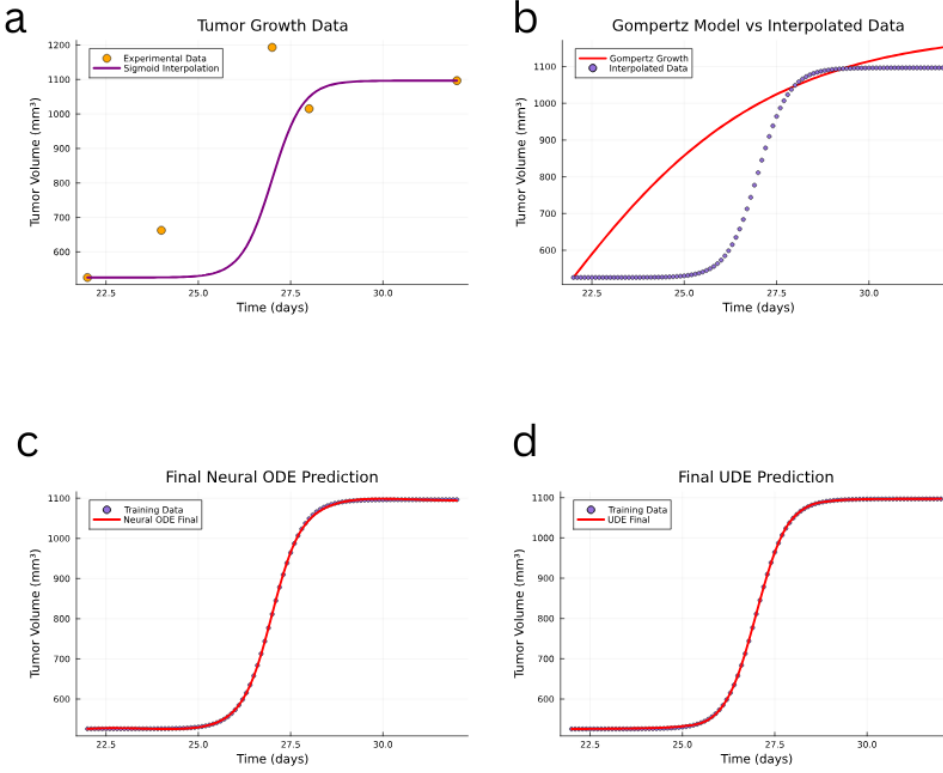


Figure 10: Plots for ID=3. (a) Sigmoid interpolation. (b) Solution to Gompertz ODE against interpolated data. (c) Solution to Neural ODE. (d) Solution to UDE.

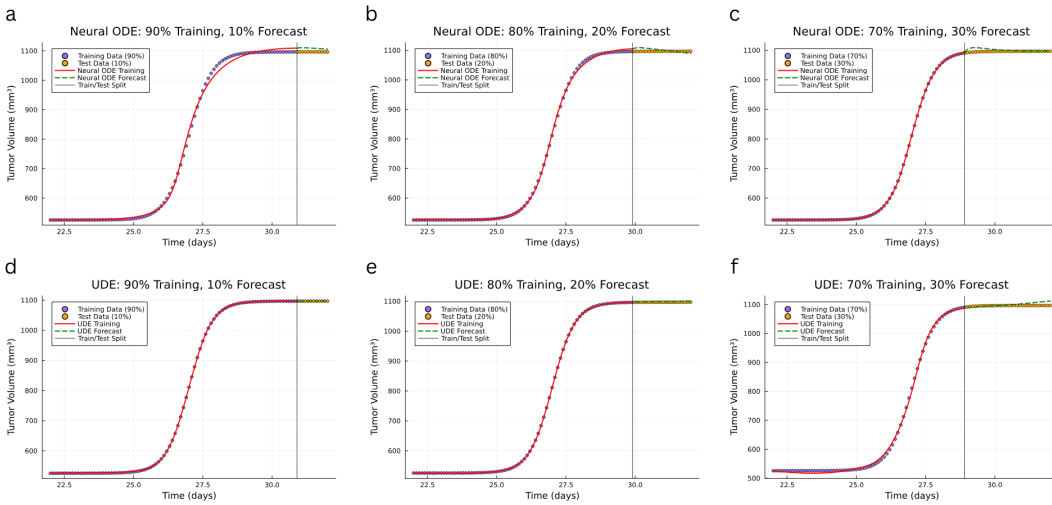


Figure 11: Forecast plots for ID=3. (a) Neural ODE forecast for 90-10 split. (b) Neural ODE forecast for 80-20 split. (c) Neural ODE forecast for 70-30 split. (d) UDE forecast for 90-10 split. (e) UDE forecast for 80-20 split. (f) UDE forecast for 70-30 split.

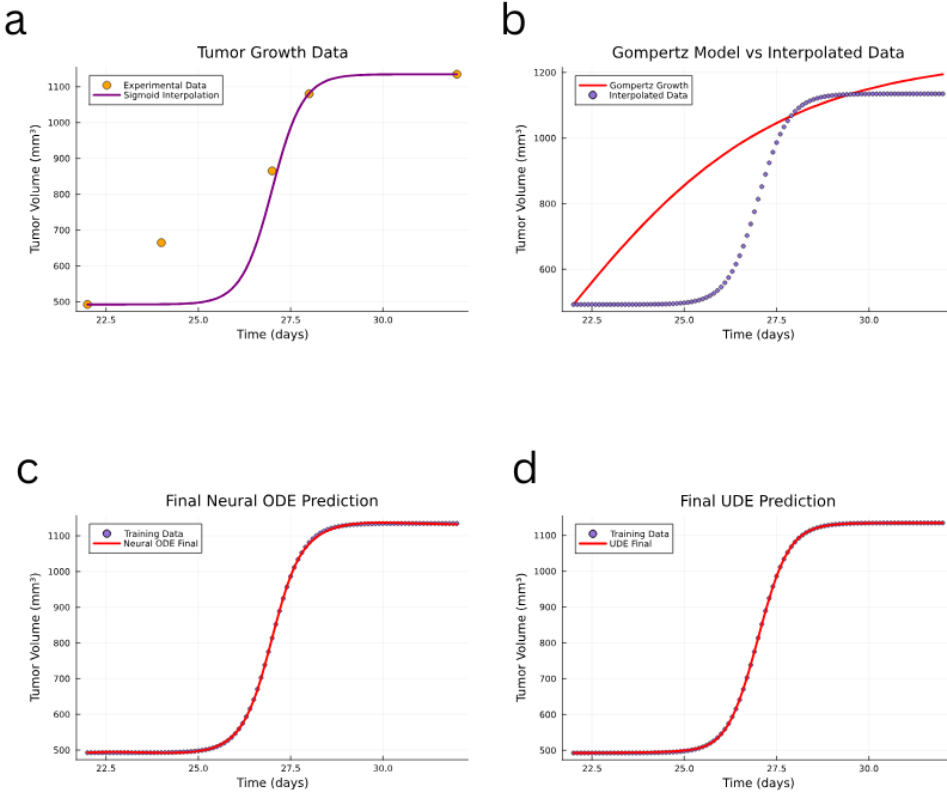


Figure 12: Plots for ID=4. (a) Sigmoid interpolation. (b) Solution to Gompertz ODE against interpolated data. (c) Solution to Neural ODE. (d) Solution to UDE.

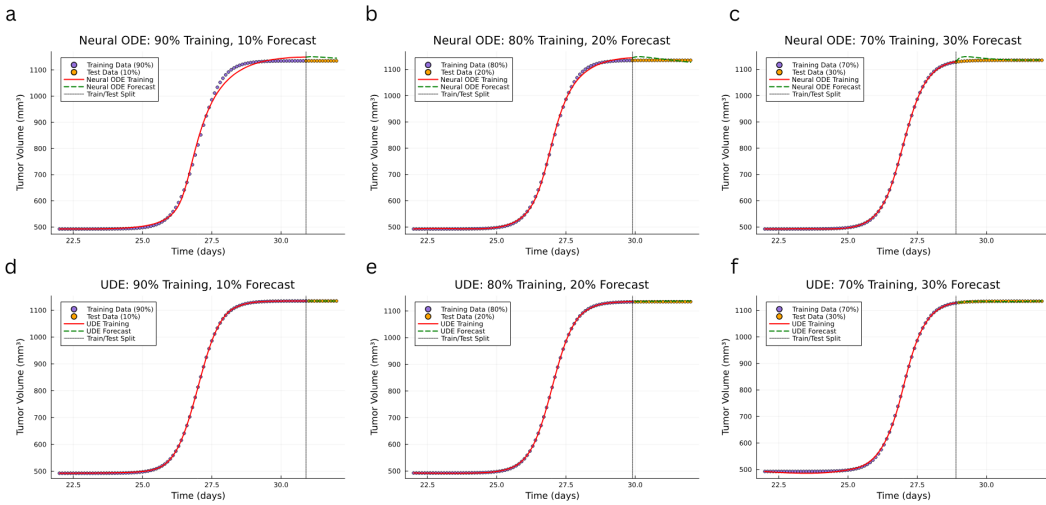


Figure 13: Forecast plots for ID=4. (a) Neural ODE forecast for 90-10 split. (b) Neural ODE forecast for 80-20 split. (c) Neural ODE forecast for 70-30 split. (d) UDE forecast for 90-10 split. (e) UDE forecast for 80-20 split. (f) UDE forecast for 70-30 split.

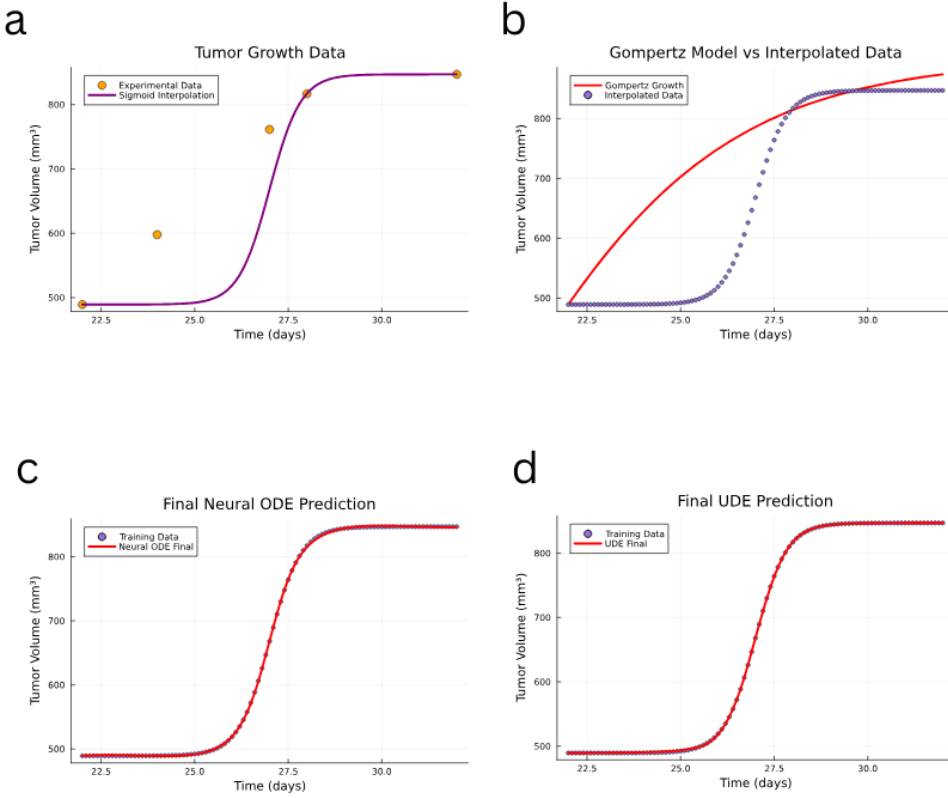


Figure 14: Plots for ID=5. (a) Sigmoid interpolation. (b) Solution to Gompertz ODE against interpolated data. (c) Solution to Neural ODE. (d) Solution to UDE.

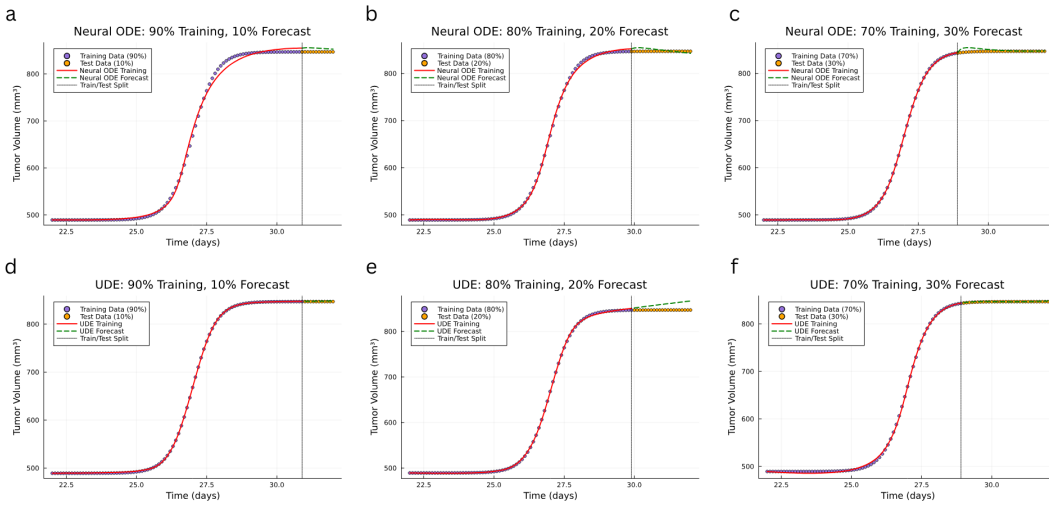


Figure 15: Forecast plots for ID=5. (a) Neural ODE forecast for 90-10 split. (b) Neural ODE forecast for 80-20 split. (c) Neural ODE forecast for 70-30 split. (d) UDE forecast for 90-10 split. (e) UDE forecast for 80-20 split. (f) UDE forecast for 70-30 split.

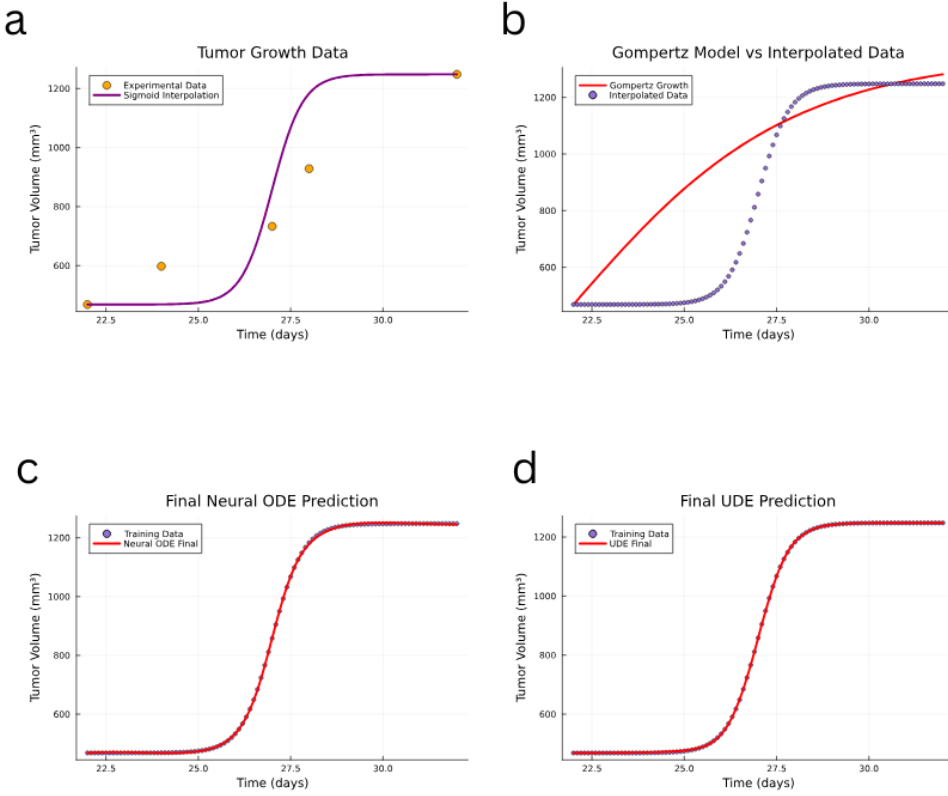


Figure 16: Plots for ID=6. (a) Sigmoid interpolation. (b) Solution to Gompertz ODE against interpolated data. (c) Solution to Neural ODE. (d) Solution to UDE.

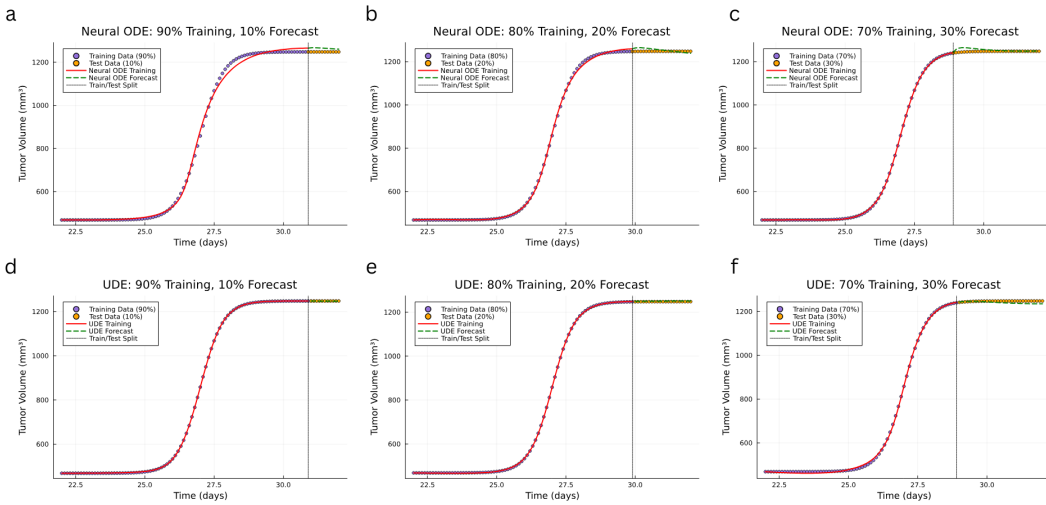


Figure 17: Forecast plots for ID=6. (a) Neural ODE forecast for 90-10 split. (b) Neural ODE forecast for 80-20 split. (c) Neural ODE forecast for 70-30 split. (d) UDE forecast for 90-10 split. (e) UDE forecast for 80-20 split. (f) UDE forecast for 70-30 split.

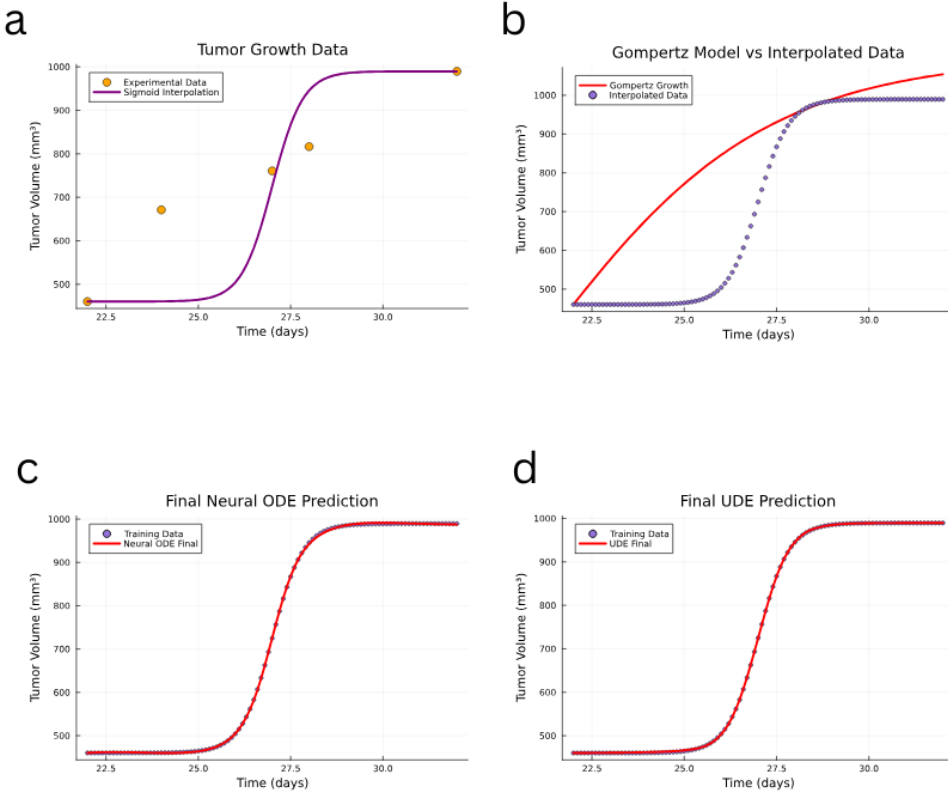


Figure 18: Plots for ID=7. (a) Sigmoid interpolation. (b) Solution to Gompertz ODE against interpolated data. (c) Solution to Neural ODE. (d) Solution to UDE.

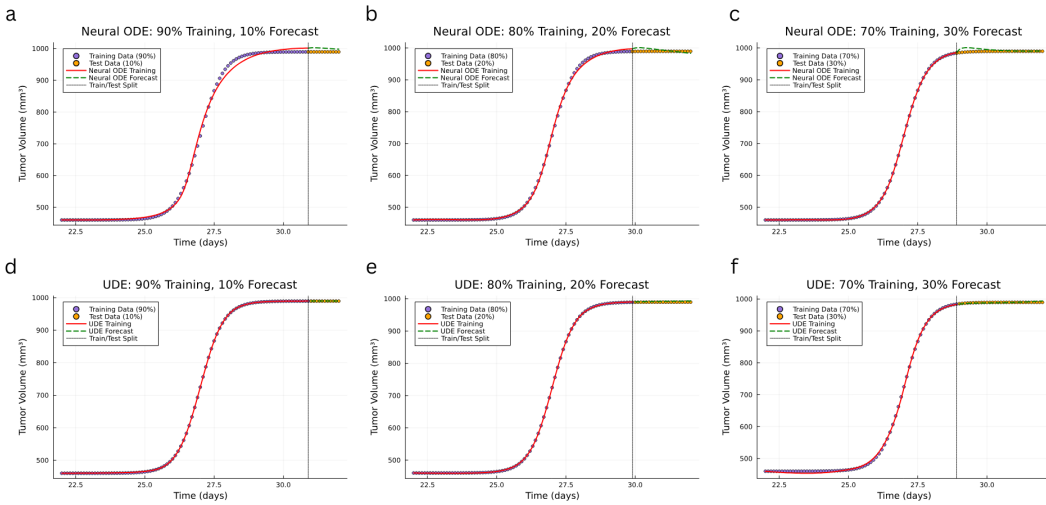


Figure 19: Forecast plots for ID=7. (a) Neural ODE forecast for 90-10 split. (b) Neural ODE forecast for 80-20 split. (c) Neural ODE forecast for 70-30 split. (d) UDE forecast for 90-10 split. (e) UDE forecast for 80-20 split. (f) UDE forecast for 70-30 split.

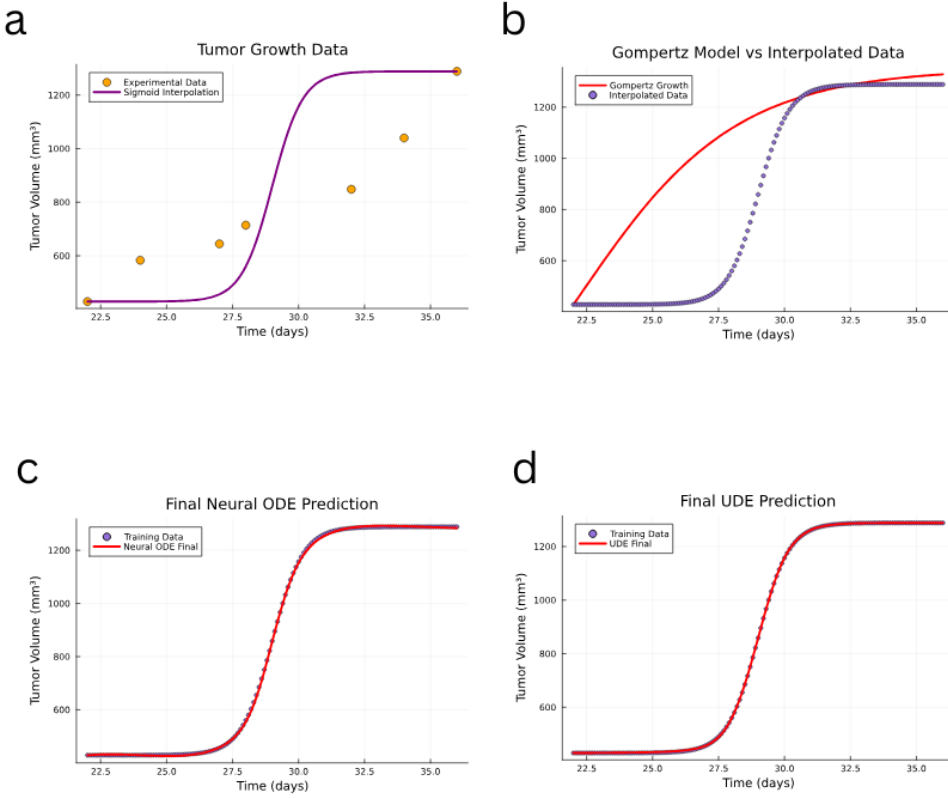


Figure 20: Plots for ID=8. (a) Sigmoid interpolation. (b) Solution to Gompertz ODE against interpolated data. (c) Solution to Neural ODE. (d) Solution to UDE.

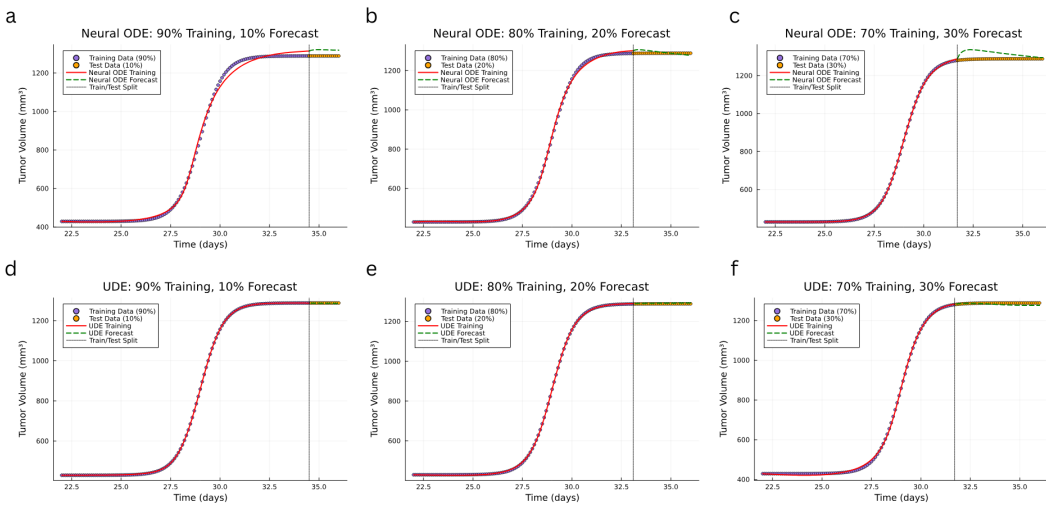


Figure 21: Forecast plots for ID=8. (a) Neural ODE forecast for 90-10 split. (b) Neural ODE forecast for 80-20 split. (c) Neural ODE forecast for 70-30 split. (d) UDE forecast for 90-10 split. (e) UDE forecast for 80-20 split. (f) UDE forecast for 70-30 split.

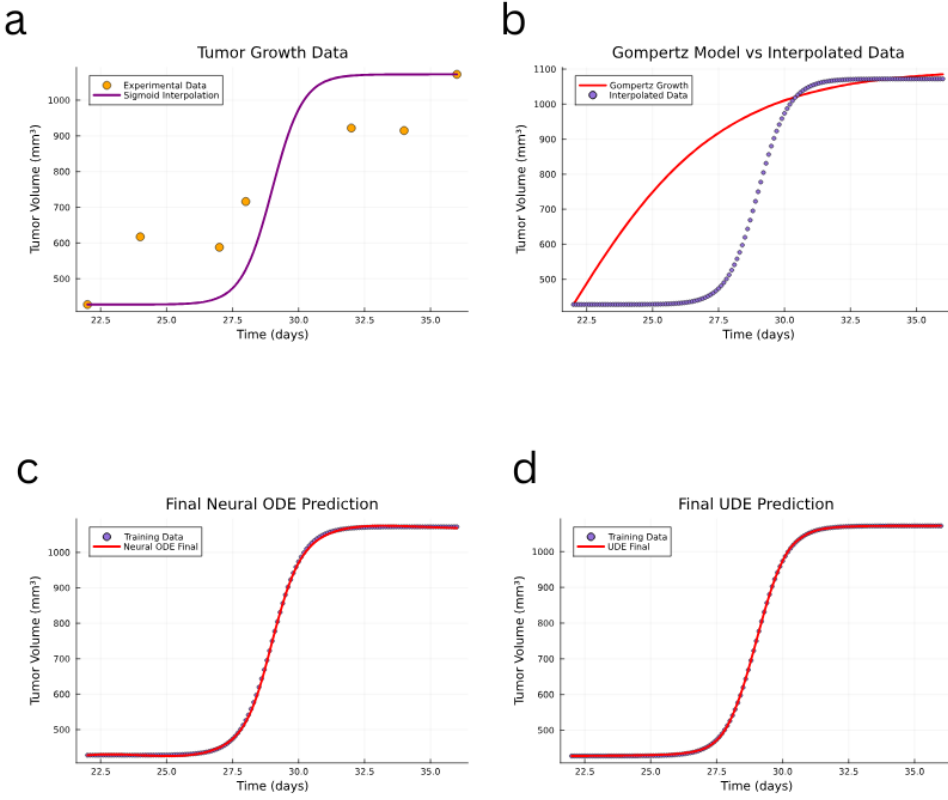


Figure 22: Plots for ID=9. (a) Sigmoid interpolation. (b) Solution to Gompertz ODE against interpolated data. (c) Solution to Neural ODE. (d) Solution to UDE.

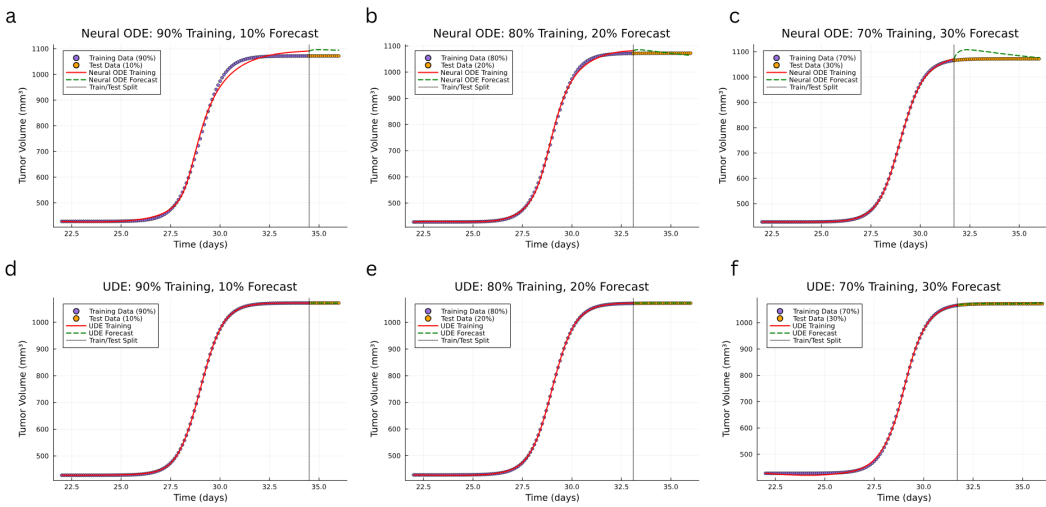


Figure 23: Forecast plots for ID=9. (a) Neural ODE forecast for 90-10 split. (b) Neural ODE forecast for 80-20 split. (c) Neural ODE forecast for 70-30 split. (d) UDE forecast for 90-10 split. (e) UDE forecast for 80-20 split. (f) UDE forecast for 70-30 split.

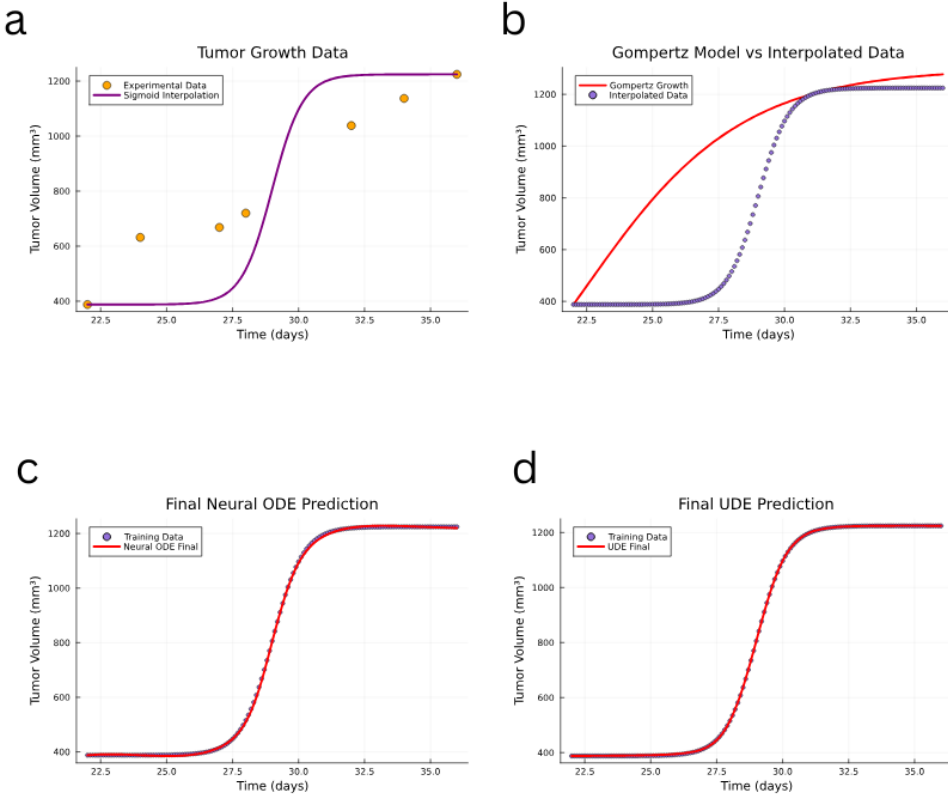


Figure 24: Plots for ID=10. (a) Sigmoid interpolation. (b) Solution to Gompertz ODE against interpolated data. (c) Solution to Neural ODE. (d) Solution to UDE.

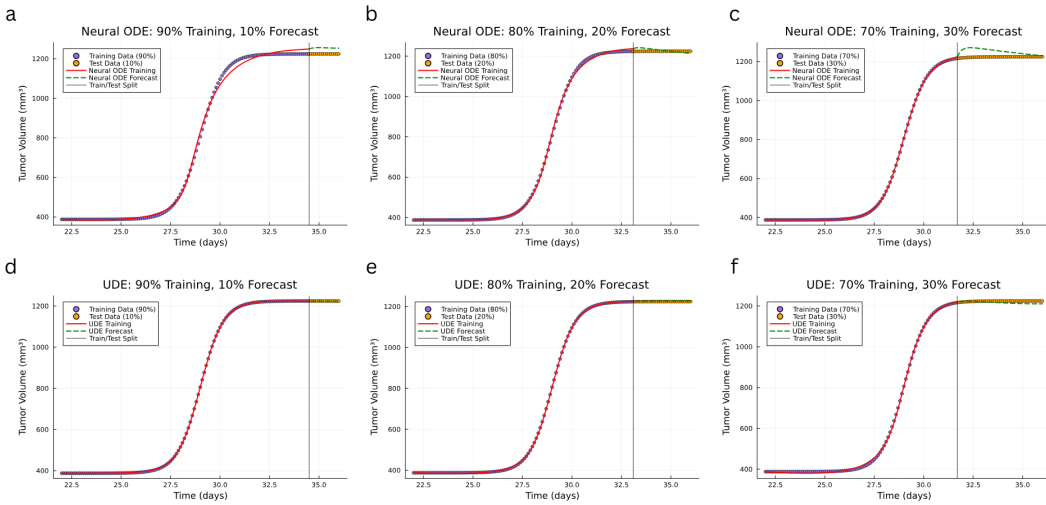


Figure 25: Forecast plots for ID=10. (a) Neural ODE forecast for 90-10 split. (b) Neural ODE forecast for 80-20 split. (c) Neural ODE forecast for 70-30 split. (d) UDE forecast for 90-10 split. (e) UDE forecast for 80-20 split. (f) UDE forecast for 70-30 split.